Evaluation of Surface Mounted PM Machine's Parameters on Load Conditions Using Frozen Permeability Method. Part. I

G. T. de Paula, J. R. B. de A. Monteiro, *Member, IEEE*, T. E. P. de Almeida, M. P. de Santana, W.C. A. Pereira.
Department of Electrical Engineering
School of Engineering of São Carlos - USP
São Carlos, Brazil
geyverson@gmail.com; jrm@sc.usp.br.

***Abstract*— This work deals with the influence of magnetic saturation on machine's parameters of a surface mounted permanent magnet synchronous machine driven by an ideal six-step three-phase inverter. In order to investigate and describe each machine's parameter, a review on Frozen Permeability Method is developed. Further, a general machine design characteristics are presented. At last, some simulation by means of finite element method with Frozen Permeability Method are carried out taking into account that the machine is driven by an ideal square current waveform. The results for line inductance, flux-linkage waveform and its harmonic contents are shown and analyzed.**

Keywords—Permanent Magnet Synchronous Machine; frozen permeability method; magnetic saturation; surface mounted; brushless DC motor.

I. INTRODUCTION

Although permanent magnet machines have been employed in numerous industrial applications, especially high torque and high efficiency applications [1]–[3], such machines have some intrinsic characteristics that need especial attention during the design process, e.g., cogging torque, torque ripple and back-EMF.

Along the past several years, numerous researches have been carried out in order to investigate the influence of the electric loading and magnetic saturation on PM machine's parameters, such as PM flux-linkage, armature flux, inductance, back-EMF, cogging torque, reluctance torque and torque ripple [4]–[14].

The task of segregation and analysis of the torque components and any other machine's parameters during the machine operation has not been easy, even though some recent methods have been either developed or improved [7], [9], [13]. The most known method to segregate and analyze the machine's parameters on load condition is the frozen permeability (FP) method that has been widely employed along the last decade [4]–[14].

The frozen permeability method linearizes the electromagnetic machine circuit around the machine operating point, i.e., the DC magnetization curve of each material is used to calculate the machine operating point and then the permeability in this point is calculated and fixed. Thus, based on the new electromagnetic machine circuit, a new simulation is carried out in order to get the desired parameter. The frozen permeability method can be used in either finite element method (FEM) or magnetic circuit model (MCM). The accuracy in FEM depends on the mesh generation and it usually takes much more time to solve the problem than MCM, however its results are better than MCM [13].

In this paper, the frozen permeability method is employed by means of finite element method in order to segregate and analyze the flux-linkage waveform and line inductance of a surface mounted permanent magnet machine. Different from previous researches [5], [9], [10], [13], where the machines are driven by an ideal sinusoidal current waveform, the machine in this paper is driven by an ideal square current waveform, i.e., by an ideal six-step three-phase inverter.

II. MAIN DIMENSIONS OF MACHINE

The surface mounted permanent magnet machine whose dimensions are shown in Table I and illustrated in Fig. 1 is simulated with frozen permeability method by means of finite element method.

TABLE I. MACHINE DIMENSIONS

Parameter	Dimension
Slot number	24
Pole number	4
Stator outer diameter	116.6 mm
Stator inner diameter	61 mm
Stator yoke width	14.35 mm
Air-gap length	1.35 mm
Rotor outer diameter	58.3 mm
Tooth width	3.52 mm

Parameter	Dimension
Slot opening	2.15 mm
Shaft diameter	19 mm
Tooth tip edge	1 mm
Magnet thickness	7.6 mm
Magnet type	NdFeB 10 MGOe (Bonded)

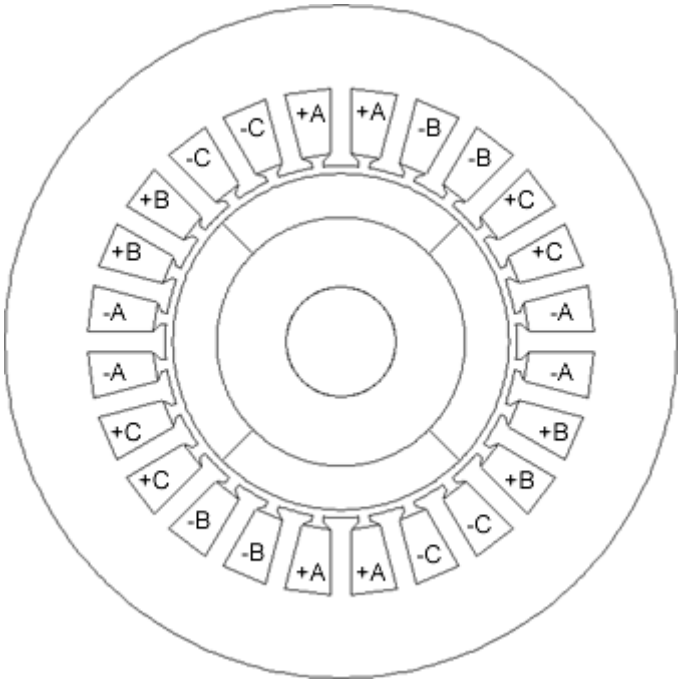

Fig. 1. Cross-section of the machine

As shown in Fig. 1, the winding schemes for one phase of the machine is [+, 0, 0, 0, 0, -, -, 0, 0, 0, 0, +, +, 0, 0, 0, 0, -, -, 0, 0, 0, 0, +].

Another characteristic, which should be taken into account, is that the stator lamination stack has no skewing slot, neither the rotor is skewed.

III. Frozen Permeability Method

Since the stator and rotor are made of nonlinear magnetic material, it is not possible to segregate the flux components – PM flux and armature flux – applying the theorem of superposition to these two sources of flux.

Thus, in order to segregate the flux components and make possible the employment of superposition theorem, the frozen permeability (FP) method is employed [5], [9], [10], [13]. The FP method linearizes the electromagnetic machine circuit around the machine operating point (*OP*), i.e., the DC magnetization curve of each material is used to calculate the machine operating point (*OP*) and then the permeability in this point is calculated and fixed (μ_{OP}) as illustrated in Fig. 2.

Once the permeability is frozen and based on the new electromagnetic machine circuit – that takes into account the value of permeability assessed on load condition –, a new simulation is carried out in order to get the contribution of each source of electromagnetic flux to the total flux.

Without the linearization proposed by FP, the sum of the flux density of each source of electromagnetic flux (B_{PM}, for permanent magnet; *Bi*, for armature) does not yield in the flux density of the operating point (B_{OP}). Although, the sum of the excitation of each source of electromagnetic flux (H_{PM}, for permanent magnet; *Hi*, for armature) yields in the excitation of the operating point (H_{OP}).

However, with the linearization proposed by FP, the sum of the flux density of each source of electromagnetic flux (B_{PM}-*FP*, for permanent magnet; *Bi-FP*, for armature) yields in the flux density of the operating point (B_{OP}). In addition, the sum of the excitation of each source of electromagnetic flux (H_{PM}, for permanent magnet; *Hi*, for armature) still yields in the excitation of the operating point (H_{OP}) [5], [9], [10], [13]. The Fig. 2 illustrates the FP method.

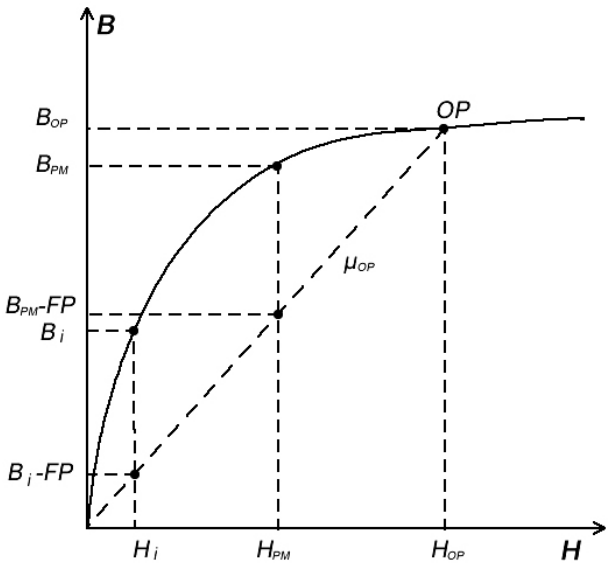

Fig. 2. Frozen Permeability Method.

IV. Six-Step Three-Phase Inverter

As mentioned, the machine in this paper is driven by an ideal square current waveform, i.e., an ideal six-step three-phase inverter. The current waveforms are shown in Fig. 3.

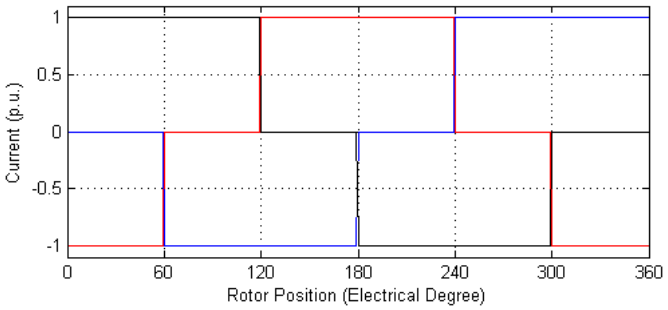

Fig. 3. Ideal Currente Waveforms.

V. No-Load Characteristics

A. Flux-Linkage

The phase A flux-linkage waveform is shown in Fig. 4 and its harmonic content is shown in Fig. 5.

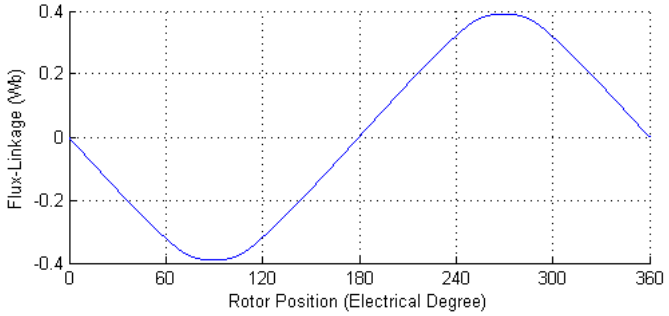

Fig. 4. No-load Flux-Linkage waveform.

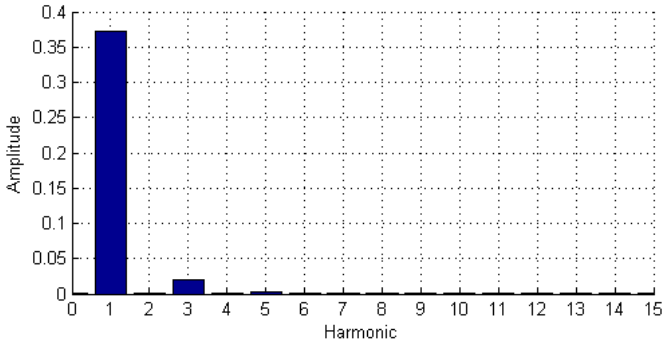

Fig. 5. Harmonic content of no-load Flux-Linkage waveform.

B. Back-EMF

The phase A Back-EMF waveform is shown in Fig. 6 and its harmonic content is shown in Fig. 7.

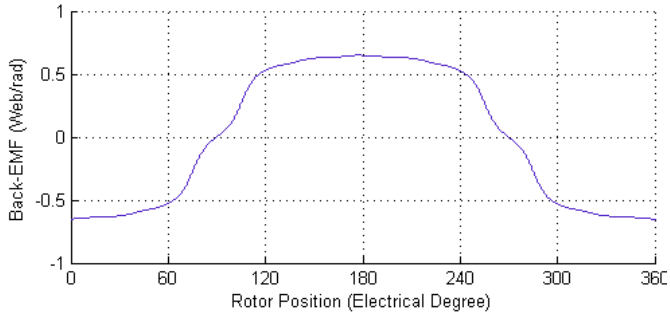

Fig. 6. No-load Back-EMF waveforms.

C. Inductance

The line-inductance value is 54.4 mH and the hypothesis under investigation in this paper deals with the behavior of this value, i.e., if it stand still 54.4 mH and does not change whereas the electrical load increases. The investigation of this hypothesis is only possible by means of frozen permeability method and the reason for this investigation lies on the fact that the surface mounted permanent magnet machine has no salience on its rotor.

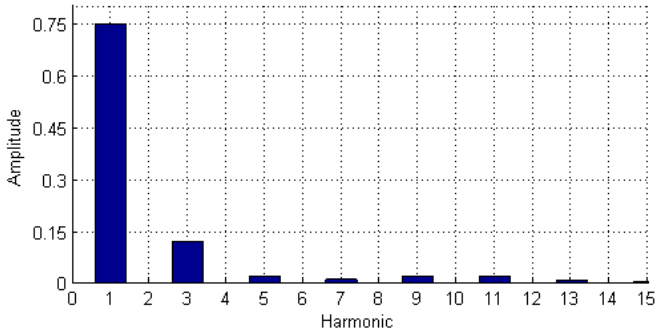

Fig. 7. Harmonic content of no-load Flux-Linkage waveform.

VI. On-Load Analysis

The machine under investigation is driven by an ideal six-step three-phase inverter, whose current waveform of each phase is shown in Fig. 3. Three different electrical load conditions are considered, 05A, 10A and 20A that represents 50%, 100% and 200%, of the nominal condition, respectively.

A. Flux Density and Field Distribution

The frozen permeability method makes possible the mathematical summation of the flux density of each source of electromagnetic flux as it is shown in Fig. 8 and 9. In Fig. 8 and 9 there are the nonlinear simulation which has PM and current as sources of flux (called “Nonlinear”); the linear simulation with only PM as source of flux (called “Linear PM”); the linear simulation with current only as source of flux (called “Linear Current”); and the linear simulation with PM and current as source of flux (called “PM + Current”).

As can be seen, the Fig. 8 shows the radial flux density whereas the Fig. 9 shows the axial flux density. These figures are an illustration of the flux contribution/decomposition and they have been made from a line along the external surface of the PM at 100% of load condition at start rotor position.

As can be noticed, the linear simulation with PM and current as source of flux yields the same result of the nonlinear simulation. The results for 50% and 200% of load condition are omitted even though their linear simulations yield the same result of their counterpart nonlinear simulation.

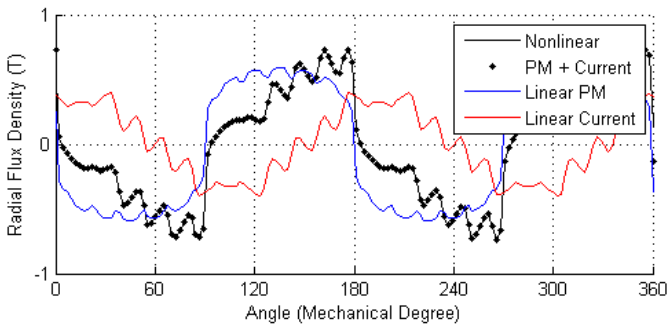

Fig. 8. Radial Flux Density at 100% of Load Condition at Start Positon.

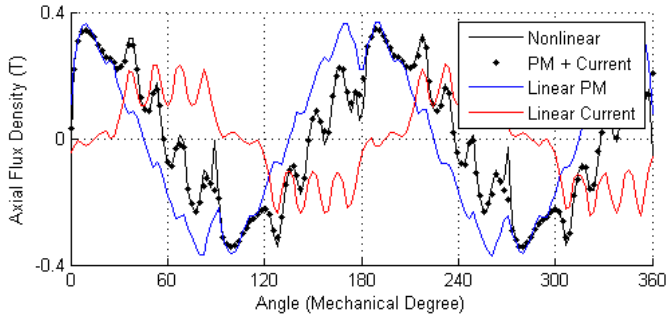

Fig. 9. Axial Flux Density at 100% of Load Condition at Start Positon.

The field contribution of each source of electromagnetic flux can be seen in Fig. 10. The nonlinear simulation is illustrated in Fig. 10(a); the linear simulation with PM and current as sources of flux (called "PM + Current") is illustrated in Fig. 10(b); the linear simulation with PM only as source of flux (called "Linear PM") is illustrated in Fig. 10(c); and the linear simulation with current only as source of flux (called "Linear Current") is illustrated in Fig. 10(d). Once again, these figures are an illustration of the field contribution and they have been made at 100% of load condition at start rotor position.

As can be noticed, the linear simulation with both PM and current as sources of flux yields the same result of the nonlinear simulation for field distribution.

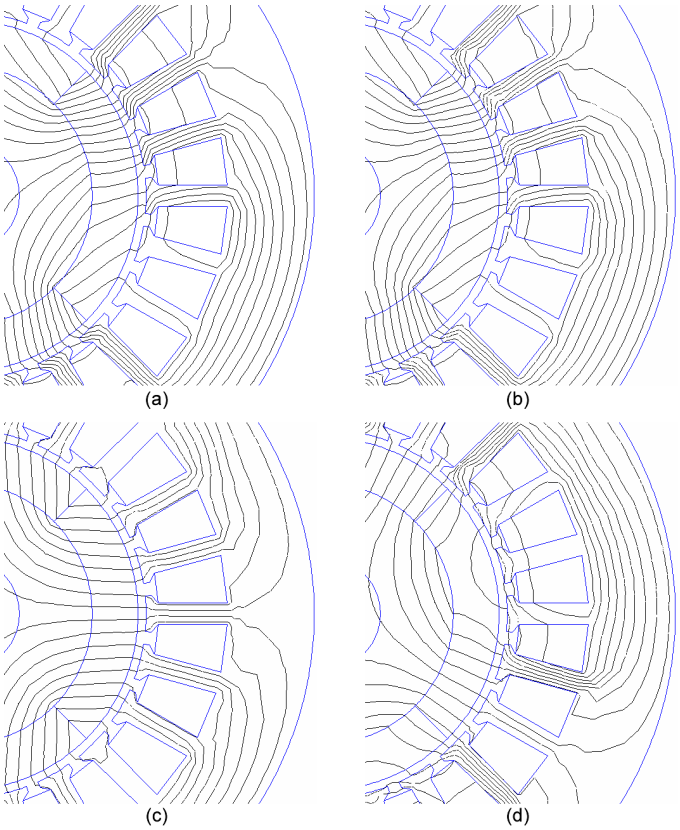

Fig. 10. Field Distribution. (a) Nonlinear simulation; (b) "PM + Current" simulation; (c) Linear PM simulation; (d) Linear Current simulation.

B. *Flux-Linkage*

The phase A flux-linkage waveforms for no load, 50%, 100% and 200% of load condition are shown in Fig. 11 and their harmonic content are shown in Fig. 13. The Fig. 12 shows a zoom in flux-linkage waveforms near flux peak value (between 240 and 300º electrical).

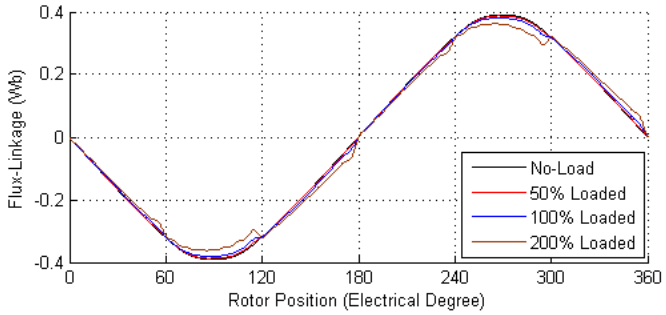

Fig. 11. Flux-Linkage waveforms for no load, 50%, 100% and 200% of load condition.

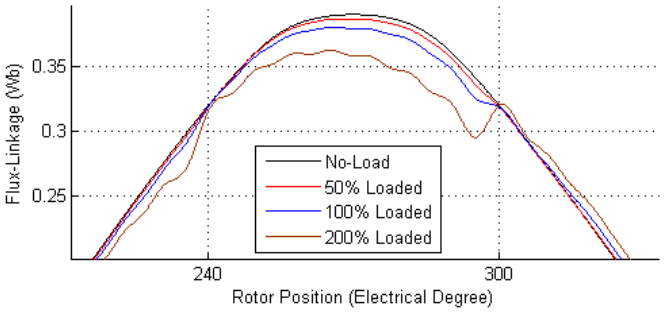

Fig. 12. Zoom in Flux-Linkage waveforms near flux peak value (between 240 and 300º electrical).

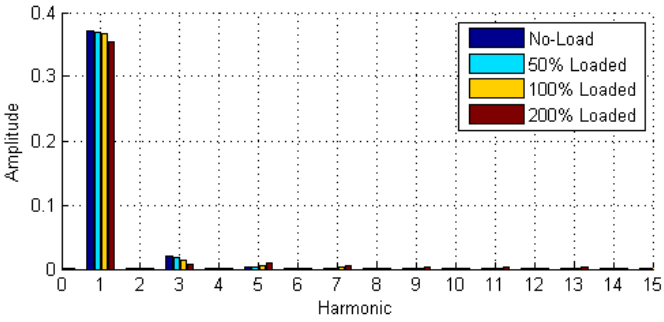

Fig. 13. Harmonic content of Flux-Linkage waveforms for no load, 50%, 100% and 200% of load condition.

Instead of being smooth as it used to be with no load, the flux-linkage gets some disturbances in its waveform when the load increases. Despite the flux-linkage getting lower, especially around the peak value, its waveform has small disturbances when the load value is lower than 100%. Over 100% of load condition such disturbances are more evident and the flux-linkage waveform gets far from the no load flux-linkage waveform as shown in Fig. 11 and 12.

The harmonic content shown in Fig. 13 shows that the fundamental and third harmonic decreases whereas the load increases. As can be noticed, the fifth and seventh harmonic increases, though.

The most noticeable disturbances in the flux-linkage waveform happen every 60º electrical. They are related to the switching of the two phases in the six-step three-phase inverter that changes the magnetic circuit behavior abruptly in the machine.

C. *Inductance*

Since the machine winding is wye connected and it is driven by a six-step three-phase inverter, only two phases are supplied in every 60º electrical period, so the line inductance is more important than the phase inductance in parameter analysis. The Fig.14 shows the line inductance waveform for 50%, 100% and 200% of load condition.

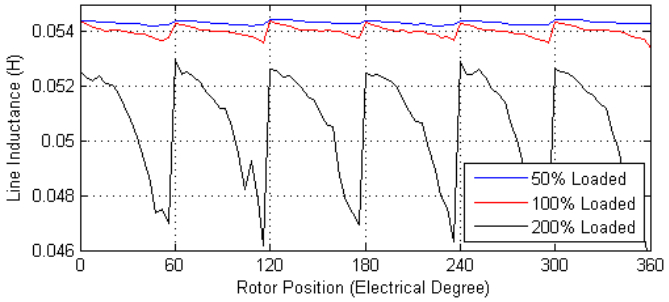

Fig. 14. Line Inductance waveforms for 50%, 100% and 200% of load condition.

As mentioned, the line inductance of no load condition is 54.4 mH and it has been considered constant. However, as shown in Fig. 14 the line inductance is not constant even though the surface mounted permanent magnet machine has no salience on its rotor. The reason for this changing lies on the fact that the teeth becomes saturated, especially the teeth shoes as can be seen in Fig. 15.

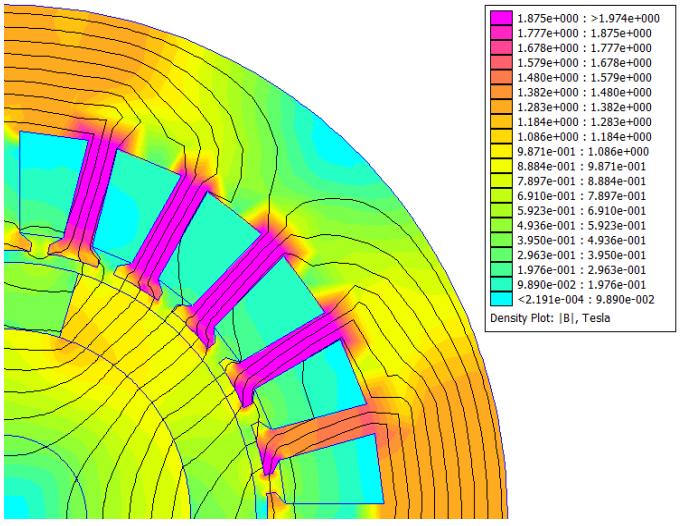

Fig. 15. Machine Teeth Saturated.

The average, minimum and maximum line inductance values decrease whereas the load increases. As can be seen, for load conditions over 100% the line inductance ripple is lower than 3%. The Fig. 16 compares the average line inductance value for each load condition and Fig. 17 compares the line inductance ripple for each load condition.

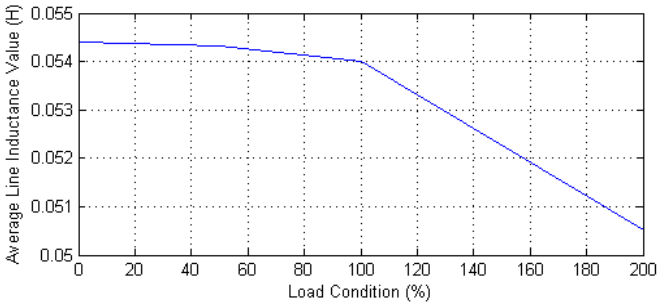

Fig. 16. Average Line Inductance value.

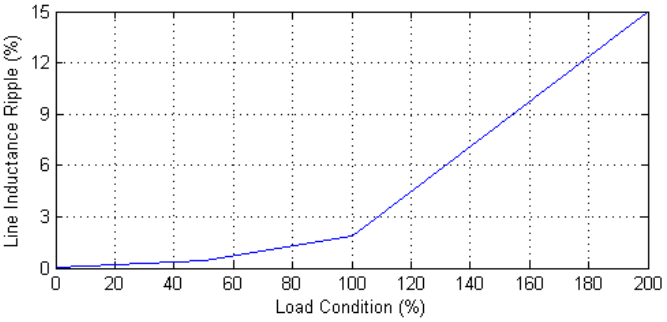

Fig. 17. Line Inductance Ripple.

In the vector control for non-sinusoidal machines proposed in [15], the quadrature axis component (called i_{qx}) has a constant value and the direct axis component (called i_{dx}) has a sawtooth waveform with period of 60º electrical for square current waveform, as employed in this paper. Comparing the line inductance of Fig. 14 with the sawtooth waveform from i_{dx} in [15] it can be noticed an inverse relationship, i.e., when the line inductance value is maximum the i_{dx} value is minimum and vice-versa. The maximum direct axis component value indicates the maximum alignment of PM flux with the armature flux provided by a square current waveform.

When the direct axis component reaches its maximum value, the line inductance reaches its minimum value due to the alignment of PM flux with the armature flux, which contributes to the saturation of the teeth and reduces the permeability of the stator. In the other hand, when the direct axis component reaches its minimum value, the line inductance reaches its maximum value due to the non-alignment of PM flux with the armature flux, which does not contribute to the saturation of the teeth and the reduction of the permeability of the stator.

VII. CONCLUSION

A surface mounted permanent magnet synchronous machine driven by an ideal square current waveform has been simulated and some of its parameters have been analyzed

employing the frozen permeability method. As explained in Section III, the frozen permeability method makes possible the employment of superposition theorem to the two sources of flux (PM flux and armature flux), even though the machine has non-linear magnetic material. The Figs. 8, 9 and 10 show the results for Radial and Axial flux density and field distribution for non-linear simulation and for the linear simulation carried out with the frozen permeability method by means of finite element method.

The machine whose dimensions and characteristics are shown in Table I and Fig. 1 has been simulated by means of finite element method with three different electrical load conditions: 5A (50%), 10A (100%) and 20A (200%).

The first parameter under investigation is the flux linkage waveform. As can be noticed in Figs 11, 12 and 13, the flux linkage waveform stood smooth for load conditions lower than 100%, although its peak value decreases. Reasonable disturbances are evident when the electrical load is over 100%.

The second parameter under investigation is the line inductance and the hypothesis of it is stand still constant over any electrical load whereas the rotor has no salience. As can be noticed in Figs 14, 16 and 17, the line inductance is reasonably affected by the magnetic saturation on teeth for load condition over 100% of nominal condition. For load conditions lower than 100% the line inductance ripple is lower than 3% and can be regardless.

Further work might investigated the Back-EMF, cogging torque, reluctance torque and mutual torque in order to estimate the electromagnetic torque.

ACKNOWLEDGMENT

The authors acknowledge the support granted by CNPQ, CAPES and FAPESP.

REFERENCES

[1] T. J. E. Miller and J. R. Hendersot Jr, Design of brushless permanent-magnet motors. Oxford University Press, 1995, p. 584.

[2] D. C. Hanselman, Brushless Permanent-Magnet Motor Design. Mcgraw-Hill, 1994, p. 191.

[3] J. F. Gieras and M. Wing, Permanent magnet motor technology: design and applications, vol. 113. CRC Press, 2002, p. 590.

[4] J. Arellano-Padilla, C. Gerada, G. Asher, and M. Sumner, "Inductance characteristics of PMSMs and their impact on saliency-based sensorless control," Proc. 14th Int. Power Electron. Motion Control Conf. EPE-PEMC 2010, pp. 1–9, Sep. 2010.

[5] Z. Azar, Z. Zhu, and G. Ombach, "Influence of Electric Loading and Magnetic Saturation on Cogging Torque, Back-EMF and Torque Ripple of PM Machines," Magn. IEEE Trans., vol. 48, no. 10, pp. 2650–2658, 2012.

[6] Z. Azar, Z. Q. Zhu, and G. Ombach, "Torque-speed performance analysis of fractional slot PM machines having concentrated windings using alternate methods," 6th IET Int. Conf. Power Electron. Mach. Drives (PEMD 2012), pp. B73–B73, 2012.

[7] N. Bianchi and S. Bolognani, "Magnetic models of saturated interior permanent magnet motors based on finite element analysis," Conf. Rec. 1998 IEEE Ind. Appl. Conf. Thirty-Third IAS Annu. Meet. (Cat. No.98CH36242), vol. 1, pp. 27–34, 1998.

[8] N. Bianchi and S. Bolognani, "Design techniques for reducing the cogging torque in surface-mounted PM motors," IEEE Trans. Ind. Appl., vol. 38, no. 5, pp. 1259–1265, Sep. 2002.

[9] W. Q. Chu and Z. Q. Zhu, "On-Load Cogging Torque Calculation in Permanent Magnet Machines," IEEE Trans. Magn., vol. 49, no. 6, pp. 2982–2989, Jun. 2013.

[10] W. Q. Chu and Z. Q. Zhu, "Average Torque Separation in Permanent Magnet Synchronous Machines Using Frozen Permeability," IEEE Trans. Magn., vol. 49, no. 3, pp. 1202–1210, Mar. 2013.

[11] M. S. Islam, S. Mir, T. Sebastian, and S. Underwood, "Design Considerations of Sinusoidally Excited Permanent-Magnet Machines for Low-Torque-Ripple Applications," IEEE Trans. Ind. Appl., vol. 41, no. 4, pp. 955–962, Jul. 2005.

[12] J. K. Tangudu, T. M. Jahns, A. M. EL-Refaie, and Z. Q. Zhu, "Lumped parameter magnetic circuit model for fractional-slot concentrated-winding interior permanent magnet machines," 2009 IEEE Energy Convers. Congr. Expo., pp. 2423–2430, Sep. 2009.

[13] J. K. Tangudu, T. M. Jahns, A. M. El-Refaie, and Z. Q. Zhu, "Segregation of torque components in fractional-slot concentrated-winding interior PM machines using frozen permeability," 2009 IEEE Energy Convers. Congr. Expo., pp. 3814–3821, Sep. 2009.

[14] E. Schmidt and M. Susic, "Parameter evaluation of permanent magnet synchronous machines with tooth coil windings using the frozen permeabilities method with the finite element analyses," 25th IEEE Can. Conf. Electr. Comput. Eng., 2012.

[15] J. R. B. A. Monteiro, A. A. Oliveira, M. L. Aguiar, and E. R. Sanagiotti, "Electromagnetic torque ripple and copper losses reduction in permanent magnet synchronous machines," Eur. Trans. Electr. Power, vol. 22, no. 5, pp. 627–644, Jul. 2012.